Available online at www.sciencedirect.com
SCIENCE DIRECT®
International Journal of Thermal Sciences 43 (2004) 1161–1169
International Journal of Thermal Sciences
www.elsevier.com/locate/ijts

3-D thermal modelling applied to stress-induced anisotropy of thermal conductivity

H. Pron *, C. Bissieux

Université de Reims, unité de thermique et analyse physique, EA 2061, laboratoire de thermophysique (URCA/UTAP/LTP), UFR Sciences, Moulin de la housse, B.P 1039, 51687 Reims cedex 2, France

Received 14 February 2003; received in revised form 5 March 2004; accepted 13 April 2004

Available online 24 June 2004

Abstract

The present work consists in the development of a three-dimensional model of heat diffusion in orthotropic media, based on numerical Fourier transforms, and taking into account the extent of the source. This model has been applied, together with a Gauss–Newton parameter estimation procedure, to identify the components of the conductivity tensor of a steel bar under uniaxial loading. Few percent variations of the conductivity components have been observed for applied stresses remaining in the elastic domain.

Keywords: Anisotropic conductivity; Mechanical stress; Thermal modelling; Lock-in detection; Photothermal thermography; Non-destructive testing

Most of the existing heat diffusion models have been developed under homogeneous, isotropic conditions. However, several applications require to take into account a possible anisotropy of the thermophysical properties. Only a few works (Degiovanni [1], Balageas [2], Pujola [3], Amazouz [4]) considering the anisotropy of the material have been realised up today, and they often consider a punctual or uniform source (see Özisik [5] and references cited therein, but also Fournier et al. [6]). On the other hand, several works deal with the anisotropy of the thermal properties in composite materials (Pan [7], Hadjov [8], Jezowski [9]), in single crystals (Smontara [10], Gusakov [11], between others), or in polymer films (Piraux [12], Newman [13]) but the relation between physical properties and stress in common solids has been rarely studied (one can quote, for example, David et al. [14]).

The aim of the present study is to propose a model taking into account both orthotropy of the thermal conductivity tensor and extent of the modulated source. This model, based on numerical spatial Fourier transforms, takes advantage of the increase of the computers capabilities: amplitude and phase maps of the response of an orthotropic medium, submitted to a modulated (non-uniform but also non-punctual) stimulation can be obtained in only a few minutes.

This model has been validated *via* a comparison with a well-known model in an axisymetrical situation. Then it has been applied to the identification of the thermal conductivity tensor components in the case of a steel sample, submitted to a uniaxial mechanical loading.

Various experimental devices have been found in the literature: optical beam deflection (Monzyk [15]), thermoreflectance (Li [16]), pulsed heating (Fournier [6]) are the most used, and infrared thermography is sometimes chosen as measurement tool of the thermal signal (Burleigh [17]). Photothermal thermography, under modulated laser stimulation at the front face of the sample, has been chose here: series of images are recorded by a focal plane array camera, and experimental amplitude and phase maps are obtained thanks to a lock-in procedure. The three-dimensional model, together with a Gauss–Newton parameter estimation procedure, allows the identification of the conductivity tensor components parallel and perpendicular to the loading. Finally, a Student's test gives confidence intervals to the identified values.

* Corresponding author. Fax: +33-3-26-91-32-50.
E-mail address: herve.pron@univ-reims.fr (H. Pron).

1290-0729/$ – see front matter
doi:10.1016/j.ijthermalsci.2004.04.006

Nomenclature

C	specific heat	$J{\cdot}kg^{-1}{\cdot}K^{-1}$
E	Young modulus	GPa
I	radiative flux	$W{\cdot}m^{-2}$
h_0, h_L	heat transfer coefficient at the front/rear face	$W{\cdot}m^{-2}{\cdot}K^{-1}$
k^x, k^y, k^z	thermal conductivity components	$W{\cdot}m^{-1}{\cdot}K^{-1}$
L	sample thickness	m
q	volumic heat source	$W{\cdot}m^{-3}$
r_0	laser beam radius at $1/e$	m
t	time	s
T, T_{amb}, T_c	temperature	K
x, y	space coordinates, in the plane of the sample surface	m
z	space coordinate, normal to the surface of the sample	m
u, v	Fourier variables associated to the space coordinates x, y	m
R	reflection coefficient	

Greek letters

α	linear expansion coefficient	K^{-1}
β	absorption coefficient	m^{-1}
ε	strain tensor	
ρ_i	density of the layer i	$kg{\cdot}m^{-3}$
ν	Poisson coefficient	
σ	stress tensor	MPa
ω	pulsation	s^{-1}

Operators and notations

X_i	quantity corresponding to the layer i
X''	component of the X quantity parallel to the surface
$X^{\perp}$	component of the X quantity perpendicular to the surface
$\overline{X}$	one-dimensional Fourier transform of the function X
$\overline{\overline{X}}$	two-dimensional Fourier transform of the function X
$\sim$	tensor superscript – $\tilde{\varepsilon}, \tilde{\sigma}$: strain and stress tensors
$\{\}, [\,]$	vector and square matrices

1. Experimental set-up

An infrared thermography equipment (CEDIP IRC 320-4LW) is used to measure the temperature rise at the front surface of a steel bar, simultaneously submitted to a static uniaxial mechanical loading and to the irradiation of a modulated laser beam. The optical device is presented on Fig. 1.

The infrared camera records series of images of the front-face of the sample; then phase and amplitude images of the complex temperature pattern are obtained by a homemade numerical lock-in procedure [18,19]. In order to obtain the absolute phase shift between the optical stimulation and the thermal response, a reference signal is recorded simultaneously to the images by means of a photodiode connected to a Data Acquisition Card synchronised with the camera (Fig. 2).

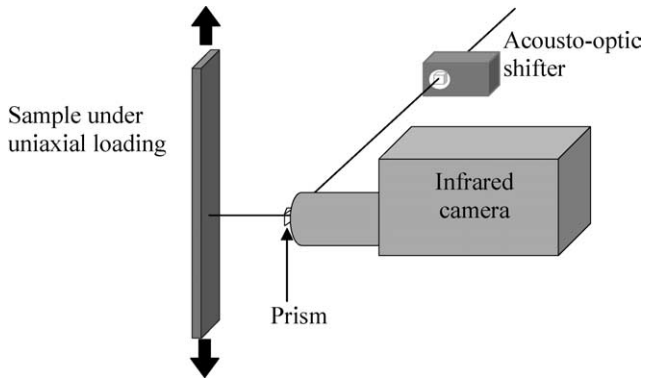

Fig. 1. Experimental set-up.

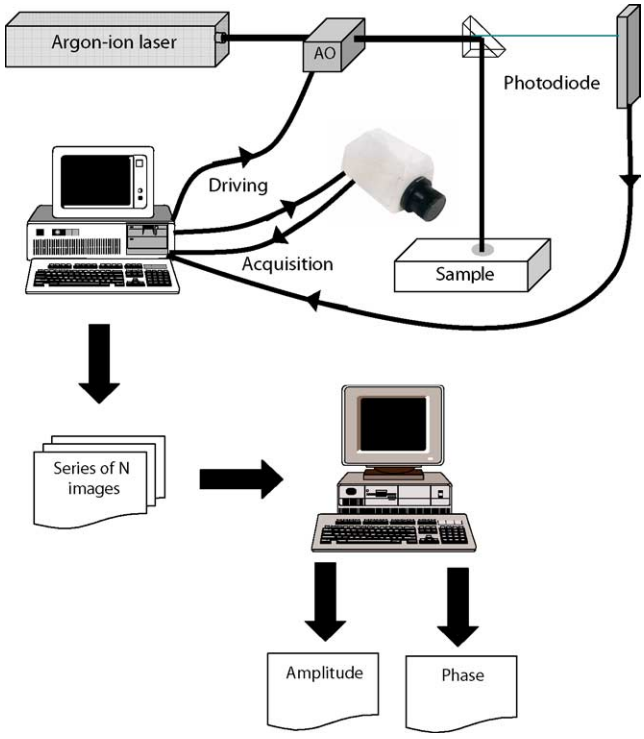

Fig. 2. Principle of the lock-in detection, with an optical reference obtain via a photodiode.

2. Three-dimensional thermal modelling

2.1. Development of the model

The present problem is to be solved in Cartesian coordinates. Since the samples are covered with black paint (in order to homogenize and enhance their emissivity), a multi-layer model is necessary; in order to remain as general as possible, we consider here p layers. If the conductivity tensor components do not depend on the position but only on the direction (orthotropic homogeneous medium), the heat equation in each layer can be written:

$$-k_i^x \frac{\partial^2 T_{i,t}}{\partial x^2} - k_i^y \frac{\partial^2 T_{i,t}}{\partial y^2} - k_i^z \frac{\partial^2 T_{i,t}}{\partial z^2} + \rho_i C_i \frac{\partial T_{i,t}}{\partial t} = q_i(x, y, z, t) \quad (1)$$

where k_i^x, k_i^y and k_i^z are the conductivity components, ρ_i the density, C_i the specific heat and $T_{i,t}$ the temperature of the layer i, and q_i the heat source in the layer i.

Under sinusoidal excitation, the time dependence of the source can be expressed as a complex exponential function, so that:

$$q_i(x, y, z, t) = q_i(x, y, z)\left(1 + e^{j\omega t}\right) \quad (2)$$

where ω is the pulsation; the temperature can then be expressed as a sum of three terms:

$$T_{i,t}(x, y, z, t) = T_{i,\text{amb}} + T_{i,c}(x, y, z) + T_i(x, y, z)e^{j\omega t} \quad (3)$$

where $T_{i,\text{amb}}$, $T_{i,c}$ and T_i are, respectively, the ambient temperature, the continuous temperature, and the thermal amplitude of the layer i. $q_i(x, y, z)$ is the spatial profile of the source, which can be separated in two components: the first one $q_i''(x, y)$ parallel to the surface and the second one $q_i^{\perp}(z)$ perpendicular (depth profile of the source):

$$q_i(x, y, z) = q_i''(x, y)q_i^{\perp}(z) \quad (4)$$

Finally, the heat equation for the alternative component can be written as follows:

$$k_i^x \frac{\partial^2 T_i}{\partial x^2} + k_i^y \frac{\partial^2 T_i}{\partial y^2} + k_i^z \frac{\partial^2 T_i}{\partial z^2} - j\omega\rho_i C_i T_i = -q_i''(x, y)q_i^{\perp}(z) \quad (5)$$

2.1.1. Fourier transforms in the plane parallel to the surface

A first Fourier transform on the x direction, applied to the heat equation as expressed before, leads to:

$$-k_i^x 4\pi^2 u^2 \overline{T_i} + k_i^y \frac{\partial^2 \overline{T_i}}{\partial y^2} + k_i^z \frac{\partial^2 \overline{T_i}}{\partial z^2} - j\omega\rho_i C_i \overline{T_i} = -\overline{q_i''}(u, y)q_i^{\perp}(z) \quad (6)$$

where $\overline{X}$ is the one-dimensional Fourier transform of the function X, and u is the Fourier variable associated to the space variable x.

Then, a Fourier transform on the y direction, leads to:

$$-k_i^x 4\pi^2 u^2 \overline{\overline{T_i}} - k_i^y 4\pi^2 v^2 \overline{\overline{T_i}} + k_i^z \frac{\partial^2 \overline{\overline{T_i}}}{\partial z^2} - j\omega\rho_i C_i \overline{\overline{T_i}} = -\overline{\overline{q_i''}}(u, v)q_i^{\perp}(z) \quad (7)$$

where $\overline{\overline{X}}$ is the two-dimensional Fourier transform of the function X and v is the Fourier variable associated to the space variable y.

Let

$$\sigma_i^2 = \frac{k_i^x}{k_i^z} 4\pi^2 u^2 + \frac{k_i^y}{k_i^z} 4\pi^2 v^2 + j\omega \frac{\rho_i C_i}{k_i^z}$$

the heat conduction equation can be resumed as follows:

$$\frac{\partial^2 \overline{\overline{T_i}}(u, v, z)}{\partial z^2} - \sigma_i^2 \overline{\overline{T_i}}(u, v, z) = -\frac{\overline{\overline{q_i''}}(u, v)}{k_i^z} q_i^{\perp}(z) \quad (8)$$

and has to be solved for the remaining spatial variable z (depth).

2.1.2. Resolution of the radiative transfer equation along the depth of the material

On the one hand, the general solutions of the associated homogeneous equation can be written as:

$$\overline{\overline{T_i}}(u, v, z) = A_i e^{-\sigma_i z} + B_i e^{\sigma_i z} \quad (9)$$

On the other hand, a particular solution, similar to the source term, has to be found (cf. [20] and [21]). In the case of a semi-transparent non-scattering medium, one can consider, in each layer i, two radiative fluxes I_i^+ and I_i^+, respectively transmitted and reflected relatively to I_0 (see Fig. 3). These fluxes must check the equation of radiative transfer in the two particular directions of the system (towards z and $-z$):

$$\frac{\partial I_i^+(z)}{\partial z} + \beta_i I_i^+(z) = 0 \quad \text{and}$$
$$\frac{\partial I_i^-(z)}{\partial z} - \beta_i I_i^-(z) = 0 \quad (10)$$

The solutions of these equations can be written as:

$$I_i^+(z) = P_i e^{-\beta_i z} \quad \text{and} \quad I_i^-(z) = M_i e^{\beta_i z} \quad (11)$$

Then, the radiative source can be expressed as the divergence of the net radiative flux:

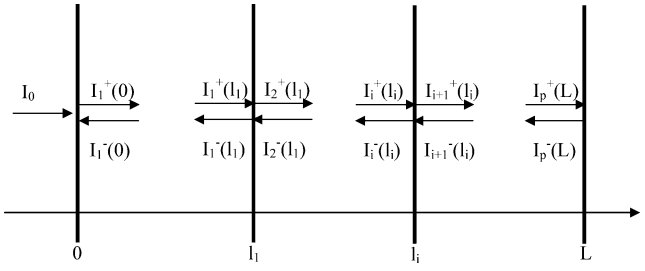

Fig. 3. Radiative fluxes in each layer.

$$q_i^{\perp}(z) = -\frac{\partial}{\partial z}\left(I_i^+ - I_i^-\right) = \beta_i\left(P_i e^{-\beta_i z} + M_i e^{\beta_i z}\right) \tag{12}$$

The coefficients P_i and M_i can be determined *via* the radiative boundary conditions:

$$\begin{cases} \text{at } z=0: & I_1^+(0) - R_0 I_1^-(0) = I_0(1-R_0) \\ \text{at } z=l_1: & -R_1 I_1^+(l_1) + I_1^-(l_1) - (1-R_1) I_2^-(l_1) = 0 \\ \text{and} & -(1-R_1) I_1^+(l_1) + I_2^+(l_1) - R_1 I_2^-(l_1) = 0 \\ & \vdots \\ \text{at } z=l_i: & -r_1 I_i^+(l_i) + I_i^-(l_i) - (1-R_i) I_{i+1}^-(l_i) = 0 \\ \text{and} & -(1-R_i) I_i^+(l_i) + I_{i+1}^+(l_i) - R_i I_{i+1}^-(l_i) = 0 \\ & \vdots \\ \text{at } z=\mathrm{L}: & -R_p I_p^+(L) + I_p^-(L) = 0 \end{cases} \tag{13}$$

Globally, $(2p)$ boundary conditions are to be written, leading to $(2p)$ equations. As far as 2 coefficients are to be determined for each layer, the resulting $2p$ coefficients can be readily calculated.

The system is expressed in matrix form, with:

$$\begin{Bmatrix} P_i \\ M_i \end{Bmatrix} = \begin{Bmatrix} P_1 \\ M_1 \\ \vdots \\ P_p \\ M_p \end{Bmatrix} \quad \text{and} \quad \{I\} = \begin{Bmatrix} (1-R_0)I_0 \\ 0 \\ \vdots \\ 0 \end{Bmatrix} \tag{14}$$

so that: $[X]\left\{\begin{smallmatrix} P_i \\ M_i \end{smallmatrix}\right\} = \{I\}$, and the coefficients P_i and M_i are completely determined after inversion of the matrix:

$$\begin{Bmatrix} P_i \\ M_i \end{Bmatrix} = [X]^{-1}\{I\} \tag{15}$$

2.1.3. Resolution of the heat diffusion equation along the depth of the material

Now, a particular solution of the equation can be written:

$$\overline{\overline{T_i}}(u,v,z) = D_i(u,v)\left[P_i e^{-\beta_i z} + M_i e^{\beta_i z}\right]\overline{\overline{q_i''}}(u,v) \tag{16}$$

so that the equation for the particular solution is:

$$\beta_i^2\overline{\overline{T_i}} - \sigma_i^2\overline{\overline{T_i}} = -\frac{\beta_i}{2k_i^z}\left(P_i e^{-\beta_i z} + M_i e^{\beta_i z}\right)\overline{\overline{q_i''}}(u,v) \tag{17}$$

The factor 2 takes into account the mean value of the sinusoidal source.

Then, the value of D_i is obviously:

$$D_i = -\frac{\beta_i}{2k_i^z(\beta_i^2 - \sigma_i^2)}$$

Finally, the particular solution is:

$$\begin{aligned} \overline{\overline{T_i}}(u,v,z) &= -\frac{\beta_i}{2k_i^z(\beta_i^2-\sigma_i^2)}\left(P_i e^{-\beta_i z} + M_i e^{\beta_i z}\right)\overline{\overline{q_i''}}(u,v) \\ &= \left[-E_i e^{-\beta_i z} - F_i e^{\beta_i z}\right]\overline{\overline{q_i''}}(u,v) \end{aligned} \tag{18}$$

And the general depth-profile of temperature, expressed in the Fourier space, is:

$$\overline{\overline{T_i}}(u,v,z) = \left(A_i e^{-\sigma_i z} + B_i e^{\sigma_i z} - E_i e^{-\beta_i z} - F_i e^{\beta_i z}\right)\overline{\overline{q_i''}}(u,v) \tag{19}$$

As far as the P_i and M_i coefficients have been determined previously, the E_i and F_i are easily determined. Then, for each layer, the A_i and B_i are to be determined *via* the conductive boundary conditions:

At the front face $(z=0)$:

$$-k_1^z \frac{\partial\overline{\overline{T}}}{\partial z}\Big|_{z=0} = -h_0\overline{\overline{T}}(0)$$

At each interface ($(p-1)$ relations of this kind):

$$-k_i^z \frac{\partial\overline{\overline{T_i}}}{\partial z}\Big|_{z=l_i} = -k_{i+1}^z \frac{\partial\overline{\overline{T_{i+1}}}}{\partial z}\Big|_{z=l_i}$$

And ($(p-1)$ relations of this kind):

$$\overline{\overline{T_i}}(l_i) = \overline{\overline{T_{i+1}}}(l_i)$$

At the rear face $(z=L)$:

$$-k_p^z \frac{\partial\overline{\overline{T}}}{\partial z}\Big|_{z=L} = h_L\overline{\overline{T}}(L)$$

These boundary conditions lead to the following system:

$$\begin{cases} \left(k_1^z\sigma_1 + h_0\right)A_1 - \left(k_1^z\sigma_1 - h_0\right)B_1 \\ \quad = \left(h_0 + k_1^z\beta_1\right)E_1 + \left(h_0 - k_1^z\beta_1\right)F_1 \\ k_i^z\sigma_i A_i e^{-\sigma_i l_i} - k_i^z\sigma_i B_i e^{\sigma_i l_i} - k_{i+1}^z\sigma_{i+1}A_{i+1}e^{-\sigma_{i+1}l_i} \\ \qquad + k_{i+1}^z\sigma_{i+1}B_{i+1}e^{\sigma_{i+1}l_i} \\ \quad = k_i^z\beta_i E_i e^{-\beta_i l_i} - k_i^z\beta_i F_i e^{\beta_i l_i} - k_{i+1}^z\beta_{i+1}E_{i+1}e^{-\beta_{i+1}l_i} \\ \qquad + k_{i+1}^z\beta_{i+1}F_{i+1}e^{\beta_{i+1}l_i} \quad i \in \{1,2,\ldots,p-1\} \\ A_i e^{-\sigma_i l_i} + B_i e^{\sigma_i l_i} - A_{i+1}e^{-\sigma_{i+1}l_i} - B_{i+1}e^{\sigma_{i+1}l_i} \\ \quad = E_i e^{-\beta_i l_i} + F_i e^{\beta_i l_i} - E_i e^{-\beta_{i+1}l_i} \\ \qquad - F_{i+1}e^{\beta_{i+1}l_i} \quad i \in \{1,2,\ldots,p-1\} \\ \left(k_p^z\sigma_p - h_L\right)e^{-\sigma_p L}A_p - \left(k_p^z\sigma_p + h_L\right)e^{\sigma_p L}B_p \\ \quad = \left(k_p^z\beta_p - h_L\right)e^{-\sigma_p L}E_p - \left(k_p^z\beta_p + h_L\right)e^{\sigma_p L}F_p \end{cases} \tag{20}$$

that can also be written in matrix form:

$$[M]\begin{Bmatrix} A_i \\ B_i \end{Bmatrix} = \{S\} \tag{21}$$

where $[M]$ is the $2p \times 2p$ matrix of the coefficients (in terms of k_i, β_i, σ_i, u, v and h) and $\{S\}$ is a vector matrix issued from the source elements (functions of E_i and F_i), and composed with the terms of the right members of the system.

The A_i and B_i coefficients are finally obtained by inversion of the matrix M:

$$\begin{Bmatrix} A_i \\ B_i \end{Bmatrix} = [M]^{-1}\{S\} \tag{22}$$

2.1.4. Inverse Fourier transforms

In the case of a laser excitation, the radial profile of the source is gaussian and expressed as:

$$q_i''(x,y) = e^{-\frac{(x^2+y^2)}{r_0^2}} \tag{23}$$

The double Fourier transform of this source is gaussian:

$$\overline{\overline{q_i''}}(u,v) = \sqrt{\pi}\, r_0 e^{-\pi^2 r_0^2 (u^2+v^2)} \tag{24}$$

And the complete expression of the complex bi-dimensional Fourier transform of the temperature distribution is:

$$\overline{\overline{T_i}}(u,v,z) = \left(A_i e^{-\sigma_i z} + B_i e^{\sigma_i z} - E_i e^{-\beta_i z} - F_i e^{\beta_i z}\right) \times \sqrt{\pi}\, r_0 e^{-\pi^2 r_0^2 (u^2+v^2)} \tag{25}$$

The last step consists in a double inverse Fourier transform, and finally the complex temperature distribution is:

$$T_i(x,y,z) = TF^{-1}\left[\left(A_i e^{-\sigma_i z} + B_i e^{\sigma_i z} - E_i e^{-\beta_i z} - F_i e^{\beta_i z}\right) \times \sqrt{\pi}\, r_0 e^{-\pi^2 r_0^2 (u^2+v^2)}\right] \tag{26}$$

2.2. Influence of the conductivity tensor orthotropy on the amplitude and phase maps

The direct model has been preliminary validated by comparison with an axisymetrical one [20], under identical conditions. Then, its sensibility to the principal components of the conductivity tensor has been studied. Figs. 4 and 5 show that the differences between the maps are very slight, even if the variation of the conductivity tensor components is wide (50% in this case). On that account, an efficient estimation procedure is necessary to identify, from such maps, the corresponding variations of the conductivity tensor components. However, it is possible to note that the phase maps are slightly more sensible to these variations than the amplitude ones.

In the experimental work presented hereafter, owing to calculation limitations, only two perpendicular phase profiles across the laser beam, corresponding to the direction parallel to the loading and to the direction perpendicular to it, have been considered.

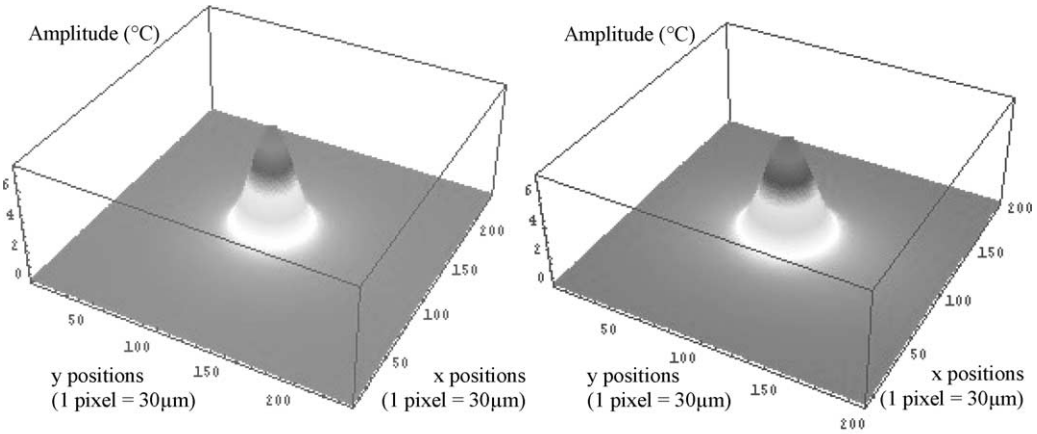

$k_x = k_y = k_z = 30$ $k_x = 20\ ;\ k_y = k_z = 40$

Fig. 4. Influence of the orthotropic conductivity on the amplitude maps.

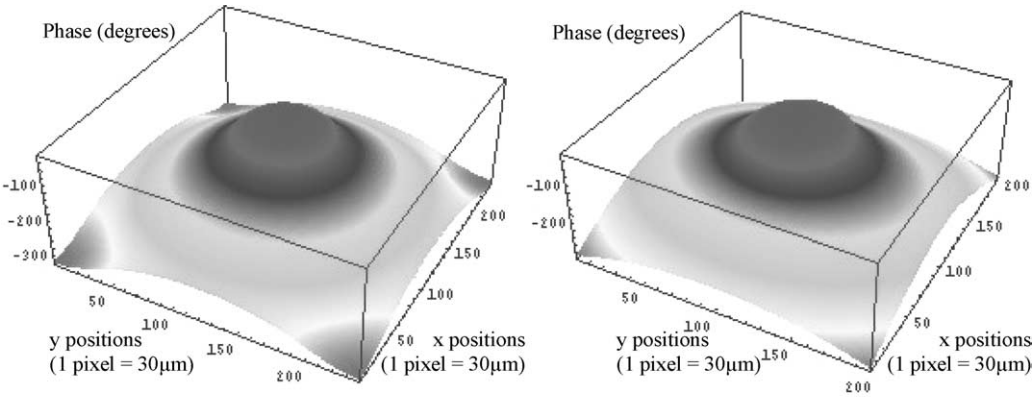

$k_x = k_y = k_z = 30$ $k_x = 20\ ;\ k_y = k_z = 40$

Fig. 5. Influence of the orthotropic conductivity on the phase maps.

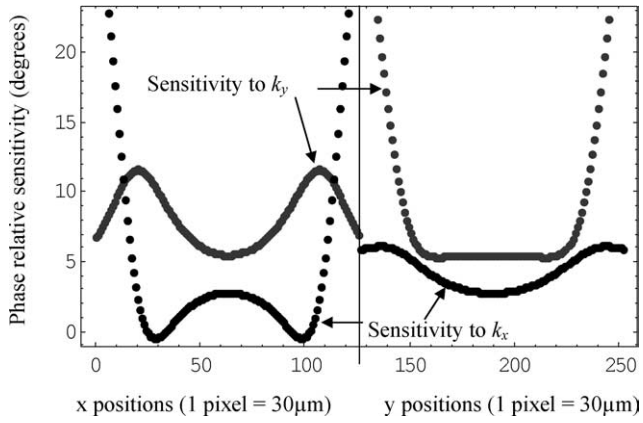

Fig. 6. Phase relative sensitivity to the conductivity tensor components along x and y axis.

The use of only two perpendicular profiles could seem to be a waste of data, since the whole amplitude and phase maps are available: only 400 measurements are taken into account though 40 000 are stored during the experiment. However, one can note that, under these conditions, the gaussian profile of the laser beam is over-sampled so that the two profiles used contain enough information to allow the identification of the researched parameters.

Consequently, in case of a smaller source point (focused laser beam, for example), the same procedure could be applied, but using the whole map in order to compensate the worse sampling of the source; this allows us to consider that the technique has not yet reached its limits in terms of spatial resolution.

The sensitivity of these phase profiles to the k_x and k_y components of the thermal conductivity tensor has been studied. The results are presented on Fig. 6: as far as the sensitivity profiles are quite different according to the considered direction, it seems to be possible to separate the influence of the two components of the conductivity tensor in the plane of the surface.

3. Application to stress-induced thermal anisotropy

3.1. Expected variations of the conductivity tensor components

As far as the considered applied stresses are uniaxial, the strain tensor ε can be expressed as follows:

$$\varepsilon = \begin{pmatrix} \frac{\sigma}{E} & 0 & 0 \\ 0 & -\nu\frac{\sigma}{E} & 0 \\ 0 & 0 & -\nu\frac{\sigma}{E} \end{pmatrix} \tag{27}$$

The "thermal" main directions being the same as the "mechanical" ones, the conductivity tensor can thus be written:

$$\tilde{k} = \begin{pmatrix} k_{11} & 0 & 0 \\ 0 & k_{22} & 0 \\ 0 & 0 & k_{33}=k_{22} \end{pmatrix} = \begin{pmatrix} k_x & 0 & 0 \\ 0 & k_y & 0 \\ 0 & 0 & k_z=k_y \end{pmatrix} \tag{28}$$

The expected variations of the thermal conductivity tensor components can be estimated through their dependence on the temperature *via* the Hooke–Duhamel law. Actually, the variations of the thermophysical properties, like those of any observable property, can be expressed as a function of the partial derivatives relative to each state variable of the system. The state variables involved here are the strain tensor and the temperature.

For a tensorial quantity like thermal conductivity, the calculation must be carried out for each component:

$$\mathrm{d}k_{ij} = \left(\frac{\partial k_{ij}}{\partial T}\right)_{\varepsilon} \mathrm{d}T + \sum_{kl}\left(\frac{\partial k_{ij}}{\partial \varepsilon_{kl}}\right)_{T,\,\varepsilon\neq\varepsilon_{kl}} \mathrm{d}\varepsilon_{kl} \tag{29}$$

Starting from an isotropic state to another, the variations of the thermal conductivity components in the main directions are:

$$\begin{aligned}\Delta k_{ii} &= \left(\frac{\partial k_{ii}}{\partial T}\right)_{\varepsilon} \Delta T + \sum_{kk}\left(\frac{\partial k_{ii}}{\partial \varepsilon_{kk}}\right)_{T,\,\varepsilon\neq\varepsilon_{kk}} \varepsilon_{kk} \\ &= \left[\left(\frac{\partial k_{ii}}{\partial T}\right)_{\varepsilon} + \sum_{k}\left(\frac{\partial k_{ii}}{\partial \varepsilon_{kk}}\right)_{T,\,\varepsilon\neq\varepsilon_{kk}} \alpha\right]\Delta T\end{aligned} \tag{30}$$

In fact, the thermal expansion coefficient α becomes a tensor; however its variations remain small and are neglected here.

However, the variation of a given conductivity component must be distinguished, either the strain component is parallel or perpendicular to the conductivity component.

The measured variation of the conductivity as a function of the temperature is not sufficient to evaluate all the partial derivatives, giving only the sum of the derivatives along the parallel and the two perpendicular directions together with that relative to the temperature.

$$\begin{aligned}&\left(\frac{\Delta k}{\Delta T}\right)_{\text{experimental}} \\ &\quad = \alpha\left(\frac{\partial k_{ii}}{\partial \varepsilon_{ii}}\right)_{\varepsilon\neq\varepsilon_{ii}} + 2\alpha\left(\frac{\partial k_{ii}}{\partial \varepsilon_{kk}}\right)_{\varepsilon\neq\varepsilon_{kk}} + \left(\frac{\partial k}{\partial T}\right)_{\varepsilon}\end{aligned} \tag{31}$$

Nevertheless, the last term seems particularly difficult to be measured. Indeed, the sample would be supposed to heat without any volume expansion.

In the case of a uniaxial stress, and without any temperature influence, the variations of the principal components are:

$$\begin{aligned}\Delta k_{11} &= \frac{\sigma}{E}\left[\left(\frac{\partial k_{11}}{\partial \varepsilon_{11}}\right) - \nu\left(\frac{\partial k_{11}}{\partial \varepsilon_{22}}\right) - \nu\left(\frac{\partial k_{11}}{\partial \varepsilon_{33}}\right)\right] \\ &= \frac{\sigma}{E}\left[\left(\frac{\partial k_{11}}{\partial \varepsilon_{11}}\right) - 2\nu\left(\frac{\partial k_{11}}{\partial \varepsilon_{22}}\right)\right]\end{aligned} \tag{32}$$

$$\begin{aligned}\Delta k_{22} = \Delta k_{33} &= \frac{\sigma}{E}\left[\left(\frac{\partial k_{22}}{\partial \varepsilon_{11}}\right) - \nu\left(\frac{\partial k_{22}}{\partial \varepsilon_{22}}\right) - \nu\left(\frac{\partial k_{22}}{\partial \varepsilon_{33}}\right)\right] \\ &= \frac{\sigma}{E}\left[(1-\nu)\left(\frac{\partial k_{22}}{\partial \varepsilon_{11}}\right) - \nu\left(\frac{\partial k_{22}}{\partial \varepsilon_{22}}\right)\right]\end{aligned} \tag{33}$$

Only conductivity components measurements could allow the evaluation of all the partial derivatives. However, in order

to get at least an order of magnitude, the cross derivatives are neglected here.

Then, for a carbon steel ($E = 200$ GPa, $\nu = 0.3$, $\alpha = 12 \times 10^{-6}$, $1/k(\partial k/\partial T) = -10^{-3}$ K^{-1}, see Rouby and Blanchard [22]) under a 100 MPa uniaxial stress, the variations of the conductivity components would be:

$$\frac{\Delta k_{11}}{k_{11}} = \frac{1}{\alpha E}\left(\frac{1}{k}\frac{\Delta k}{\Delta T}\right)_{\text{exp}} \approx -4.2\%$$

k being an arbitrary component, and

$$\frac{\Delta k_{22}}{k_{22}} = -\nu\frac{\Delta k_{11}}{k_{11}} \approx 1.3\%$$

However crude, these estimations lead us to expect few percent variations of the principal conductivity components for stress levels remaining within the elastic domain. One can also note that these estimations concern one kind of steel and only one. Actually, the behaviour of a stainless steel is often very different from that of a carbon steel: $\partial k/\partial T$ is often positive for the first and negative for the second. Not only the amplitude but also the sign of the conductivity variations widely depend on the considered material.

Moreover, for a given kind of material, the purity has a great influence. Finally, these estimations only allow to expect *a priori* the order of magnitude for the sensitivity of the experimental device.

A similar estimation would lead to one order of magnitude lower relative variations of the specific heat (Pron et al. [23]); this estimation is coherent with those found in the literature (see, for example, Dunn et Sparrow [24], Bridgman [25]). Thus, specific heat is considered as constant in the present work.

3.2. Experimental results

The lock-in procedure gives amplitude and phase images as presented in Fig. 7(a) and (b). One can note that the noise is really low; this is due both to the high efficiency of our home-made lock-in procedure and to the high performance of the FPA camera.

Two profiles across the laser beam (one parallel to the stress, the other along the perpendicular direction) are extracted from the experimental phase maps. Then, the identification of the parallel and perpendicular components of the conductivity tensor k_{11} and k_{22} is realised by fitting these profiles with the specially developed 3D heat diffusion model.

Fig. 8 shows how slight the differences between phase profiles without and with loading are, observation that is coherent with the expected variations.

Fig. 9 presents the variation of the parallel and perpendicular components of the thermal conductivity for a steel bar under an uniaxial loading remaining in the elastic domain. The confidence intervals are evaluated by means of a Student's test (Beck and Arnold [26], Giri [27] or Marquardt [28]), with a risk of 10%.

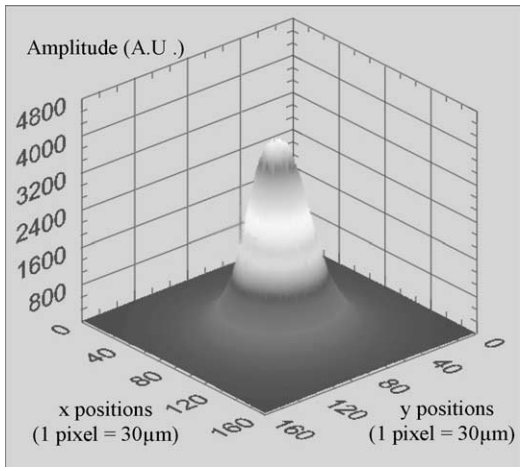

(a)

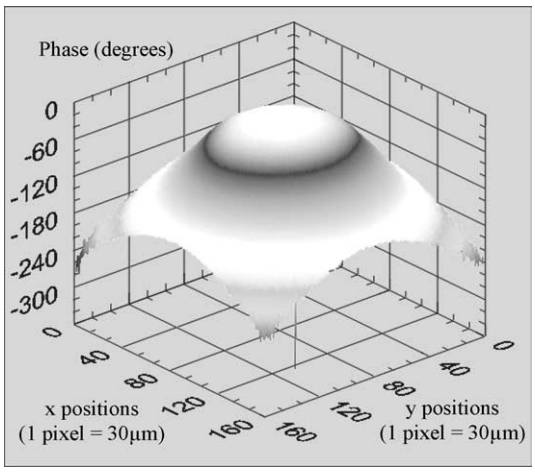

(b)

Fig. 7. (a) Amplitude image across the laser beam; (b) Phase image across the laser beam.

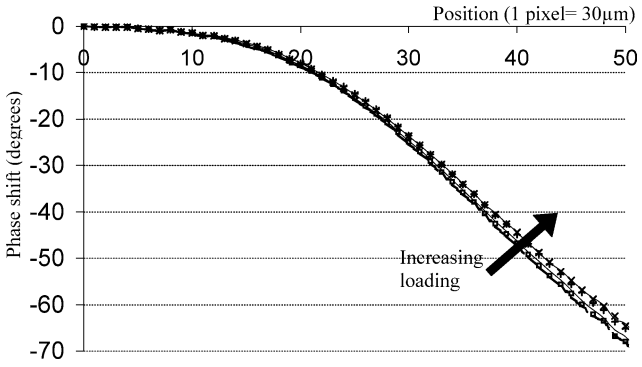

Fig. 8. Variation of a phase profile as a function of the applied stress (AISI 304).

Fig. 10 allows to state positively that our procedure is efficient since there is a good agreement between the experimental phase profiles and the profiles rebuilt with the identified components of the thermal conductivity tensor. Moreover, the procedure is able to adjust the profiles even if they are affected by a slight irregularity of the laser shape.

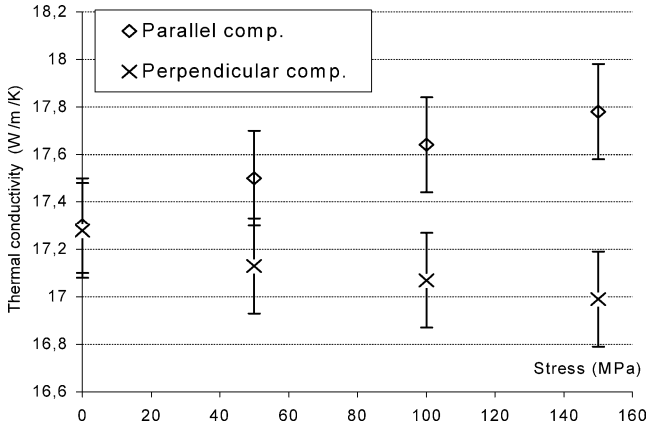

Fig. 9. Evolution of the thermal conductivity components as a function of uniaxial applied stress.

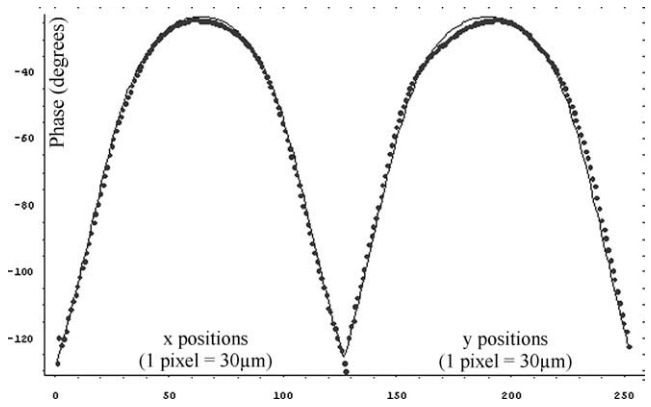

Fig. 10. Adjustment of the x and y experimental phase profiles by the theoretical 3D model.

4. Conclusions

Photothermal infrared thermography is applied here to estimate the variations of the thermal conductivity tensor components induced by a static uniaxial loading on a steel sample.

A specific three-dimensional model, based on numerical Fourier transforms, and taking into account both the stress-induced orthotropy of the medium and the extent of the source has been developed. On the experimental point of view, a specific device has been realised, allowing the application of a static uniaxial loading and, simultaneously, the irradiation of the surface by a modulated laser beam. Series of images have been recorded thanks to a focal plane array infrared camera, and experimental amplitude and phase maps are obtained thanks to a home-made lock-in procedure. After a validation of this model *via* a comparison, in an axisymetrical situation, with a well-known model, it has been applied, together with a parameter estimation procedure, to identify the conductivity tensor components in the directions parallel and perpendicular to the mechanical loading.

The obtained variations of the conductivity tensor components rather agree with the order of magnitude crudely estimated from their temperature dependence. These observations allow to consider that this procedure could lead to a complementary tool in stress analysis: the variations of the thermal conductivity being actually linked with the stress level, photothermal measurements could be a new kind of stress gauge.

Finally, it is important to note that, even if the resolution of this technique, in terms of detectable stress variations, is not really high, it is to compare with the one of existing methods: most of them are not really more accurate, and the others are intrusive or need a meticulous preparation.

References

[1] A. Degiovanni, J.C. Batsale, D. Maillet, Panorama des techniques développées au LEMTA pour la mesure de diffusivité longitudinale de matériaux anisotropes, J. Étude Soc. Française Therm. 8 (1995).
[2] D. Balageas, Détermination de la diffusivité thermique du milieu homogène équivalent à un matériau composite à renforcement orienté, C. R. Acad. Sci. Paris, Ser. II 299 (4) (1984).
[3] R.M. Pujola, D. Balageas, Derniers développements de la méthode flash adaptée aux matériaux composites à renforcement orienté, High Temperatures – High Pressures 17 (1985) 623–632.
[4] M. Amazouz, C. Moyne, A. Degiovanni, Measurement of the thermal diffusivity of anisotropic materials, High Temperatures – High Pressures 19 (1987) 37–41.
[5] M.N. Özisik, Heat Conduction, Wiley, New York, 1993.
[6] D. Fournier, K. Plamann, Thermal measurements on diamond and related materials, Diamond Related Materials 4 (1995) 809–819.
[7] C.T. Pan, H. Hocheng, Evaluation of anisotropic thermal conductivity for unidirectional FRP in laser machining, Composites Part A: Appl. Sci. Manufact. 32 (11) (2001) 1657–1667.
[8] K. Hadjov, Effective thermal conductivity tensors of composite materials with arbitrary texture, Internat. J. Thermal Sci. 42 (4) (2003) 407–416.
[9] A. Jezowski, K. Rogacki, T. Puig, X. Obradors, Anisotropy of the thermal conductivity of melt-textured Y123/Y211 composites, Physica B: Condensed Matter, Part 1 284–288 (2000) 1015–1016.
[10] A. Smontara, I. Tkalcec, A. Bilusic, M. Budimir, H. Berger, Anisotropy of the thermal conductivity in (TaSe4)2I, Physica B: Condensed Matter 316–317 (2002) 279–282.
[11] V. Gusakov, A. Jezowski, S. Barilo, N. Kalanda, A. Saiko, Anisotropy of thermal conductivity in YBaCuO single crystals, Physica C: Superconductivity, Part 3 341–348 (2000) 1867–1868.
[12] L. Piraux, E. Ducarme, J.-P. Issi, D. Begin, D. Billaud, Thermal conductivity of oriented polyacetylene films, Synthetic Metals 41 (1–2) (1991) 129–132.
[13] P.R. Newman, M.D. Ewbank, C.D. Mauthe, M.R. Winkle, W.D. Smolyncki, The temperature dependence and anisotropy of the thermal conductivity in polyacetylene, Solid State Commun. 40 (11) (1981) 975–978.
[14] C. David, B. Menéndez, M. Darot, Influence of stress-induced and thermal cracking on physical properties and microstructure of La Peyratte granite, I, J. Rock Mech. Mining Sci. 36 (1999) 433–448.
[15] J.W. Monzyk, K. Lafdi, K.W. Johnson, Thermal diffusivity measurements of carbon materials using optical beam deflection, Carbon 38 (9) (2000) 1351–1359.
[16] B. Li, L. Pottier, J.P. Roger, D. Fournier, K. Watari, K. Hirao, Measuring the anisotropic thermal diffusivity of silicon nitride grains by thermoreflectance microscopy, J. European Ceramic Soc. 19 (8) (1999) 1631–1639.
[17] D. Burleigh, W. De La Torre, Thermographic analysis of the anisotropy in the thermal conductivity of composite materials, Ther-

mosense XIII, Orlando, Florida (United States), 3–5 April, 1991, vol. 1467, pp. 303–310.
[18] H. Pron, J.F. Henry, S. Offermann, C. Bissieux, J.L. Beaudoin, Analysis of stress influence on thermal diffusivity by photothermal infrared thermography, Proceedings of QIRT '98, Lodz, 7–10 September 1998.
[19] J.-C. Krapez, Compared performances of four algorithms used for modulation thermography, Proceedings of QIRT '98, Lodz, 7–10 Septembre 1998.
[20] F. Potier, Radiométrie photothermique appliquée à la caractérisation et au contrôle du traitement thermique des métaux, Thèse, Université de Reims (1989).
[21] R. Santos, L.C.M. Miranda, Theory of the photothermal radiometry with solids, J. Appl. Phys. 52 (1981) 4194–4198.
[22] M. Rouby, P. Blanchard, Propriétés physiques et mécaniques des aciers et alliages inoxydables, in: Les Aciers Inoxydables, Les éditions de Physique, 1990, pp. 111–160.
[23] H. Pron, J.F. Henry, S. Offermann, C. Bissieux, J.L. Beaudoin, Estimation of local thermophysical properties by means of front-face photothermal infrared thermography: Application to mechanical stress analysis, High Temperatures – High Pressures 32 (2000) 473–477.
[24] S.A. Dunn, J.G. Sparrow, Stress dependance of specific heat: Observations on the TERSA technique, Strain (May 1990).
[25] P.W. Bridgman, The Effect of Pressure on the Thermal Conductivity of Metals, The Jefferson Physical Laboratory, Harvard University, Cambridge, MA.
[26] J.V. Beck, K.J. Arnold, Parameter Estimation in Engineering and Science, Wiley, New York, 1977.
[27] N.C. Giri, Introduction to Probability and Statistics, Dekker, New York, 1993.
[28] D.W. Marquardt, An algorithm for least squares estimation of nonlinear parameter, J. Soc. Indust. Appl. Mech. 2 (1963) 431–441.